HHS Public Access

Author manuscript

*Int J Eng Sci*. Author manuscript; available in PMC 2021 September 24.

Published in final edited form as:

*Int J Eng Sci*. 2020 February ; 147: . doi:10.1016/j.ijengsci.2019.103206.

# Simulation of thrombosis in a stenotic microchannel: The effects of vWF-enhanced shear activation of platelets

**Wei-Tao Wu**[1], **Mansur Zhussupbekov**[2], **Nadine Aubry**[3], **James F. Antaki**[2], **Mehrdad Massoudi**[4]

[1]School of Mechanical Engineering, Nanjing University of Science and Technology, Nanjing, J.S., 210094, China

[2]Meinig School of Biomedical Engineering, Cornell University, Ithaca, NY, 14853, USA

[3]Department of Mechanical Engineering, Northeastern University, Boston, MA, 02115, USA

[4]U. S. Department of Energy, National Energy Technology Laboratory (NETL), Pittsburgh, PA, 15236, USA

## Abstract

This study was undertaken to develop a numerical/computational simulation of von Willebrand Factor (vWF) - mediated platelet shear activation and deposition in an idealized stenosis. Blood is treated as a multi-constituent mixture comprised of a linear fluid component and a porous solid component (thrombus). Chemical and biological species involved in coagulation are modeled using a system of coupled convection-reaction-diffusion (CRD) equations. This study considers the cumulative effect of shear stress (history) on platelet activation. The vWF activity is modeled as an enhancement function for the shear stress accumulation and is related to the experimentally-observed unfolding rate of vWF. A series of simulations were performed in an idealized stenosis in which the predicted platelets deposition agreed well with previous experimental observations spatially and temporally, including the reduction of platelet deposition with decreasing expansion angle. Further simulation indicated a direct relationship between vWF-mediated platelet deposition and degree of stenosis. Based on the success with these benchmark simulations, it is hoped that the model presented here may provide additional insight into vWF-mediated thrombosis and prove useful for the development of more hemo-compatible blood-wetted devices in the future.

### Keywords

von Willebrand Factor (vWF); thrombosis; blood; platelets activation; shear stress accumulation



**Disclosure of Conflict of Interests**: The authors declare no conflict of interest.

## 1. Introduction

Hemostasis is a natural response of the body to an injury that involves a complex cascade of biochemical and fluid dynamic factors that produce a clot to prevent blood loss. However, pathological formation of blood clots (thrombosis) is responsible for many cardiovascular disorders and malfunction of blood-wetted medical devices (Furie & Furie, 2008; Handin, 2005; Stalker et al., 2013). Thrombosis involves several cascade reactions that lead to platelet activation, deposition, aggregation, and stabilization, which are also influenced by the synergistic actions of various hemodynamic and biomechanical processes (Mohan Anand & Rajagopal, 2017; Fauci, 1998; Liang et al., 2015; Lu et al., 2015; Skorczewski, Erickson, & Fogelson, 2013). Although numerous scientists and physicians have devoted years to investigating thrombosis, a quantitative understanding of the mechanical and biochemical mechanisms is far from satisfactory (Combariza, Yu, Nesbitt, Mitchell, & Tovar-Lopez, 2015; Tovar-Lopez et al., 2010). There is a critical need for improved understanding of thrombosis formation particularly under conditions of elevated shear.; this perhaps can be described through mathematical models (Ataullakhanov & Panteleev, 2005; Kuharsky & Fogelson, 2001; Sorensen, Burgreen, Wagner, & Antaki, 1999a; Wu et al., 2017).

The complete pathway of thrombus formation involves several dozens of chemical species and cascade reactions that lead to platelet activation, deposition, aggregation, stabilization, and lysis that are also influenced by synergistic action of various hemodynamic and biomechanical processes (Mohan Anand & Rajagopal, 2017; Fauci, 1998; Liang et al., 2015; Lu et al., 2015; Skorczewski et al., 2013). The large number of chemical species and the complexity of cascade reactions make it difficult to quantitatively synthesize a comprehensive picture of coagulation dynamics using traditional laboratory approaches (Kuharsky & Fogelson, 2001). This has motivated the pursuit of mathematical/computational models of thrombosis over the past three decades (M. Anand, Rajagopal, & Rajagopal, 2005; M Anand, Rajagopal, & Rajagopal, 2003, 2008; Ataullakhanov & Panteleev, 2005; Flamm et al., 2012; Fogelson, 1984; Goodman, Barlow, Crapo, Mohammad, & Solen, 2005; Sorensen et al., 1999a; Wu et al., 2017; Xu, Chen, Kamocka, Rosen, & Alber, 2008; Xu et al., 2010) to complement experimental approaches, facilitate design optimization, and generate new hypotheses (Stalker et al., 2014; Tomaiuolo et al., 2014; Wang & King, 2012; Welsh et al., 2014). The growing acceptance of computational fluid dynamics (CFD) approach for design and analysis of blood-wetted devices accentuates the need for quantitative models that can predict blood trauma and thrombosis, for example, significant and frequent complications associated with prosthetic mechanical valves (Cannegieter, Rosendaal, & Briët, 1994; Özkan et al., 2015) and continuous-flow left ventricular assist devices (cfLVADs). (Akhter, 2016; Kang et al., 2016; Muthiah et al., 2016; Netuka et al., 2016).

Great progress has been made over the past few decades by numerous investigators to develop mathematical models to simulate the process of thrombosis. However, due to the intricacies of the underlying physical and biological pathways inevitably necessitates simplifying assumptions, which limits their applicability of the models. One particular deficit is thrombosis under conditions of high shear, in which von Willebrand Factor (vWF)

plays an important role. The vWF is a large multimeric glycoprotein that acts as a bridging molecule between platelets and collagen at sites of vascular injury or other adsorbed proteins on artificial surfaces (Proudfoot, Davidson, & Strueber, 2017; Ruggeri & Jackson, 2013; Sakariassen, Bolhuis, & Sixma, 1979). If the shear stress is sufficiently great -- as found in prosthetic valves, vascular stents and ventricular assist devices -- von Willebrand factor (vWF) unfolds and facilitates platelet capture via glycoprotein Ib (GPIb) (Colace & Diamond, 2013). These bonds form rapidly and tether the platelets from being ―washed away" (Colace & Diamond, 2013; Ruggeri & Jackson, 2013; Savage & Ruggeri, 2007). This, in turn prolongs the exposure of platelets to shear, and under certain conditions, the accumulated history of shear exposure is sufficient to activate platelets, even in the absence of biochemical agonists (Peterson, Stathopoulos, Giorgio, Hellums, & Moake, 1987), or with hirudin as anticoagulant.

Motivated by the essential role of vWF in high-shear thrombosis, many studies have focused on the various mechanisms and mutual interactions with different agonists and hemodynamic conditions. Diamond (2016) (Diamond, 2016) studied the thrombus formation in microfluidic devices, where it was found that as a clot grows, shear stress can become sufficiently high to drive the self-association of vWF into massive fibers, which lead to a thrombotic occlusion. Peterson et al. (1987) (Peterson et al., 1987) found that in a vWF disaster plasma, adding vWF initiated shear-induced platelets aggregation, while in the absence of vWF or GPIb the aggregation was inhibited. Lkeda et al. (1991) (Ikeda et al., 1991) demonstrated that when vWF was present, platelets aggregation occurred at shear stresses above 80 $dyne\ cm^{-2}$ even in blood collected with hirudin as anticoagulant. This provides a possible explanation for why a stenosis with high shear stress is vulnerable to thrombosis. Nesbitt et al. (2009) (Nesbitt et al., 2009) artificially created a severe thrombosis in an injured blood vessel by creating a progressive stenosis at the injury site using a blunted needle, thus showing that platelet aggregation is primarily driven by changes in hemodynamic conditions. Furthermore, they also studied the mechanism of thrombosis in a stenosis using a microfluidic device with contraction–expansion geometries that represent pathological changes in blood vessel geometry; using a completely anti-coagulated blood, they mimicked a purely hemodynamically induced thrombosis which is mainly controlled by the vWF activity [8]. In a similar work by Westein et al. (2013) (Westein et al., 2013), the authors also demonstrated that a stenotic (plaque) geometry, which induces a high local flow rate, promotes thrombus formation due to the increased activity of vWF.

This present study was undertaken to investigate a new model of vWF-mediated thrombus formation based on the premise above. The specific objective was to replicate experimentally-observed patterns of thrombus deposition in-vitro, reported by Tovar-Lopez et al. (2010) (Tovar-Lopez et al., 2010) in stenotic microchannels, using a completely anti-coagulated blood.

## 2. Mathematical Modelling

The basic mathematical model consists of equations of motion for blood that determine the pressure and velocity fields, supplemented with a set of coupled convection-diffusion-reaction (CDR) equations that govern the transport and inter-conversion of chemical and

biological species – both within the thrombus and in the free stream (Wu et al., 2017). Following the principles of Mixture Theory, we suggest a resistive force to reflect the interaction between the fluid component (blood) and the solid component (thrombus); by assuming that the thrombus behaves like an assembly of densely packed particles (Johnson, Rajagopal, & Massoudi, 1990; Rajagopal & Tao, 1995). The activation of platelets is triggered by both chemical agonists and the cumulative effect of shear stress (history). The influence of vWF is modeled as an enhancement function for shear stress accumulation conforming to experimentally-observed unfolding rate of vWF.

### 2.1. Equations of motion for blood

Blood is treated as a multi-constituent mixture comprised of (1) a *fluid component (blood composed of RBCs-plasma)* and (2) a *thrombus component* which is treated as a porous medium here (Leiderman & Fogelson, 2011; Wu et al., 2017). The two components are coupled in a very special manner. The fluid component, i.e., blood (RBCs-plasma) is assumed to behave as a linear viscous fluid. The governing equations of motion are the conservation of mass and the linear momentum (Goodman et al., 2005; Leiderman & Fogelson, 2011; Wu et al., 2017):

$$\frac{\partial \rho}{\partial t} + div(\rho \boldsymbol{v}) = 0 \tag{1}$$

$$\rho \frac{d\boldsymbol{v}}{dt} = div\, \boldsymbol{T} + \rho \boldsymbol{b} - C_2 f(\phi)(\boldsymbol{v} - \boldsymbol{v}_T) \tag{2}$$

Where $\rho$ is the density of the fluid, $\boldsymbol{v}$ and $\boldsymbol{v}_T$ are the velocity of the fluid component and the thrombus component, respectively; $\boldsymbol{v}_T$ is related to the velocity of the bio-surface to which the thrombus attaches itself, and in this paper the bio-surface is static thus $\boldsymbol{v}_T = \frac{0m}{s}$; $\boldsymbol{b}$ is the body force; $\boldsymbol{T}$ is the Cauchy stress tensor of the fluid component, and the last term on the right hand side of Equation (2) designates a resistance force (a constitutive assumption, also known as the interaction force in mixture theory). In the above equations, *div* is the divergence operator, and $\frac{d(\,\cdot\,)}{dt}$ is the total time derivative given by

$$\frac{d(\,.\,)}{dt} = \frac{\partial(\,.\,)}{\partial t} + grad\,(\,.\,)\boldsymbol{v} \tag{3}$$

where *grad* is the gradient operator. We assume the stress tensor for the fluid component is given by:

$$\boldsymbol{T} = [\,-p(1-\phi)]\boldsymbol{I} + 2\mu(1-\phi)\boldsymbol{D} \tag{4}$$

where $p$ is the pressure (the mean stress),$\boldsymbol{I}$ is the identity tensor, $\mu$ is the shear viscosity (3.5cP) of blood, $\boldsymbol{D}$ is the symmetric part of the velocity gradient $\left[\boldsymbol{D} = 1/2\left[(grad\,\boldsymbol{v}) + (grad\,\boldsymbol{v})^T\right]\right.$. A scalar field $\boldsymbol{\phi}$ is introduced to represent the volume fraction of the deposited platelets (thrombus), see Table A5 for the definitions and the expression for $\boldsymbol{\phi}$. The density of the fluid component is given in terms of the volume fraction according to,

$\rho = (1 - \phi)\rho_0$, where $\rho_0$ is the density of the fluid component (pure RBCs-plasma suspension) (= 1060 kg/m$^3$) in the reference configuration, i.e., prior to any thrombus formation. In addition, we have ignored the effect of the thrombus formation in the continuity equation of the fluid component. The, term $C_2 f(\phi)(\boldsymbol{v} - \boldsymbol{v}_T)$ reflects the resistance on the fluid component from the thrombus, where the coefficient $C_2 = 2 \times 10^9\ kg/(m^3 s)$ is computed by assuming that the deposited platelets behave like densely compact particles (2.78um in diameter), described by Johnson et al. (Johnson, Massoudi, & Rajagopal, 1991) and Wu et al.(Wu, Aubry, & Massoudi, 2014; Wu, Aubry, Massoudi, Kim, & Antaki, 2014), and $f(\phi) = \phi(1+6.5\phi)$ is the hindrance function.

## 2.2. Convection-diffusion-reaction equations for thrombosis

The thrombosis model that we use includes seven fundamental mechanisms involved in coagulation: platelet activation, platelet deposition, thrombus propagation, thrombus dissolution or erosion, thrombus stabilization, thrombus inhibition and thrombus-fluid interaction. (See Figure 1.) Platelets are treated as a disperse medium that does not affect the physics of the flow. The model considers five categories (states) of platelets: [RP], resting platelets and [AP], activated platelets (in the flow field); deposited resting platelets, [$RP_d$], and activated platelets, [$AP_d$]; and [$AP_s$], deposited stabilized platelets. An additional five biochemical species include: [$a_{pr}$], platelet-released agonist (ADP); [$a_{ps}$], platelet-synthesized agonist (thromboxane $A_2$, $TxA_2$), which can be degraded via first-order reactions; [PT], prothrombin; [TB], thrombin, synthesized from prothrombin on the activated platelet phospholipid membrane; and [AT], anti-thrombin III, which inhibits thrombin and whose action is catalyzed by heparin. (For more information about the reaction mechanism of thrombosis, see (Fogelson & Neeves, 2015; Kuharsky & Fogelson, 2001; Sorensen et al., 1999a; Wu et al., 2017).)

The transport of the species in the flow field is described by a set of convection-diffusion-reaction equations (M. Anand et al., 2005; Kuharsky & Fogelson, 2001; Sorensen et al., 1999a; Wu et al., 2017),

$$\frac{\partial [C_i]}{\partial t} + div(\boldsymbol{v}[C_i]) = div(D_i \nabla [C_i]) + S_i \tag{5}$$

where $[C_i]$ is the concentration of species $i$; $D_i$ refers to the diffusivity of species $i$ in blood; and $S_i$ is a reaction source term for species $i$. Notice that the subscript $i$ represents the different species shown in Figure 1, rather than the traditional Einstein notation. The deposited platelets attached to the bio-surface have neither convective nor diffusive motion; therefore, in this case, Equation (4) is simplified and the deposition of platelets ([$RP_d$], [$AP_d$], and [$AP_s$]) are governed by the following concentration rate equations,

$$\frac{\partial [C_i]}{\partial t} = S_i \tag{6}$$

In Appendix A, Table A1 and Table A2 list the appropriate form for the source terms $S_i$, along with the abbreviations, and Table A3 provides the diffusion coefficients and normal concentrations for $[C_i]$. Adhesion of platelets to surfaces and all the other reactions at

a boundary are modeled by surface-flux boundary conditions, following the approach of Sorensen et al. (Sorensen et al., 1999a; Sorensen, Burgreen, Wagner, & Antaki, 1999b), which are listed in Table A4. The specific values and expressions of all the source terms and their parameters are provided in Table A5. Here, similar to the reaction terms in the internal domain, a negative flux implies consumption and a positive flux implies generation.

### 2.3. Equations of shear mediated activation of platelets

Shear activation of platelets is determined by their cumulative exposure to shear stress over time (i.e. shear history), as observed experimentally (Bodnár, 2014; Colantuoni, Heliums, Moake, & Alfrey Jr, 1977; Hellums, 1994). This is represented by the Eulerian form of the shear accumulation *(SA)* model of Anand et al. and Bodnár (M Anand et al., 2003; Mohan Anand & Rajagopal, 2002; Bodnár, 2014):

$$\frac{\partial SA}{\partial t} + div(\boldsymbol{v}SA) = f_{sa} - k_{pa}SA \tag{7}$$

where $k_{pa} = k_{apa} + k_{spa}$ is the activation rate by biochemical agonists ($k_{apa}$) and shear stress ($k_{spa}$). (See Table A1 and Table A2 for more information about the activation rates.) $div$ is the divergence operator and $\boldsymbol{v}$ is the velocity field of the fluid component (RBCs-plasma suspension). The negative sign implies the dissipation of $SA$ due to platelet activation. $f_{sa}$ defines the rate of shear stress accumulation, according to:

$$f_{sa} = \frac{1}{t_e} H(|\tau| - \tau_c) \tag{8}$$

$$H(\tau - \tau_c) = \begin{cases} 1, |\tau| \geq \tau_c \\ 0, |\tau| < \tau_c \end{cases} \tag{9}$$

which implies that the shear accumulation occurs only when the magnitude of the local shear stress, $|\tau|$, is greater than a critical level, $\tau_c$ (M Anand et al., 2003; Mohan Anand & Rajagopal, 2002; Bodnár, 2014; Colantuoni et al., 1977; Hellums, 1994). Based on Hellums (Hellums, 1994), $\tau_c$ was taken to be 50 $dynes/cm^2$. To account for the relationship between shear stress level and the exposure time observed experimentally (Anderson, Hellums, Moake, & Alfrey, 1978; Anderson, Hellums, Moake, & Alfrey Jr, 1977; Brown III, Lemuth, Hellums, Leverett, & Alfrey, 1975; Colantuoni et al., 1977; Hellums, 1994; Hung, Hochmuth, Joist, & Sutera, 1976; Johnston, Marzec, & Bernstein, 1975; Wurzinger, Opitz, Blasberg, & Schmid-Schönbein, 1985; Wurzinger, Opitz, Wolf, & Schmid-Schönbein, 1984), $t_e$ is given as:

$$t_e = 10^{\left(-2 * log_{10}^{|\tau|/\tau_r} + 5.6758\right)} \cdot s \tag{10}$$

and is plotted in Figure 2. $\tau_r = 1$ $dynes/cm^2$. The rate constant for shear stress activation $k_{spa}$ is likewise referenced to a critical value, $SA_c$:

$$k_{spa} = k_{spac} H(SA - SA_c) \tag{11}$$

$$H(SA - SA_c) = \begin{cases} 1, SA \geq SA_c \\ 0, SA < SA_c \end{cases} \quad (12)$$

Here $SA_c$ = 1.0and $k_{spa}$ is assumed to be 100 $s^{-1}$ which is derived from the time constant for morphological change of platelets exposed to shear stress (Sorensen et al., 1999a).

Figure 3 (a) depicts a representation of vWF unfolding and thrombus formation as described by Westein (REF Westein). The proposed model assumes that, if shear stress within the stenosis is sufficient to cause the vWF multimers to unfold, they bind to the adsorbed proteins on the surface, and capture nearby platelets via GP1b. Once captured, the platelets are susceptible to activation by prolonged exposure to elevated shear. Hence, the effect of the vWF is mathematically described in terms of an accelerated rate of stress accumulation, analogous to equation (8):

$$f_{sa} = \frac{1}{t_e}(1 + f_{vWF})H(\tau - \tau_c) \quad (13)$$

where $f_{vWF}$ is the *amplification function* due to the vWF. Here we adopt the function introduced by Lippok et al. (2016) (Lippok et al., 2016) and Schneider et al. (2007) (Schneider et al., 2007), based on the experimentally observed unfolding rate of vWF:

$$f_{vWF} = \frac{C_{vWF}}{1 + exp(-(\tau - \tau_{1/2})/\Delta\tau)} \quad (14)$$

where $\tau_{1/2}$ is shear stress at which half of the vWF multimers are fully unfolded, $\Delta\tau$ is the shear stress duration of the transition, and $C_{vWF}$ is the maximum achievable value of the amplification constant. This is a sigmoidal function, and is depicted in Figure 3 (normalized to $C_{vWF}$ = 1) for different values of $\Delta\tau$ which is determined by best fit to experimental data, below. The specific boundary value problem simulated in this study is depicted in Figure 3 (b) replicating the in-vitro experiment of Tovar-Lopez in which several idealized stenoses were studied (Tovar-Lopez et al., 2010). The geometry was parameterized in terms of the stenosis gap $L_c$ and expansion angle $\theta$, see Figure 3 (b). The above mathematical model was numerically implemented using an open-source finite element software library (OpenFOAM) (OpenCFD, 2011).

## 3. Results

### Effect of expansion angle ($\theta$) on vWF mediated platelet deposition

A series of simulations were performed to compare with the experiments of Tovar-Lopez et al. in stenotic channels (2010) (Tovar-Lopez et al., 2010). The entrance length was given as $L_c = 20\mu m$ and the inlet velocity was 0.0205 m/s corresponding to a Reynolds number of 0.70. Also based on the experimental protocol, platelet activation by biochemical agonists was completely inhibited (Tovar-Lopez et al., 2010). The inlet [RP] and [AP] were prescribed as $3 \times 10^{14}$ $PLTs/m^3$ and 1% of [RP] respectively (Sorensen et al., 1999a; Wu et al., 2017). Following Goodman et al. (2005) (Goodman et al., 2005) and Wu et al. (2017) (Wu et al., 2017), the characteristic embolization shear rates were $\tau_{emb}$ = 120 $dyne\ cm^{-2}$ and

$\tau_{emb} = 0.1\ dyne\ cm^{-2}$. Similar to Wu et al. (2017) (Wu et al., 2017), a comparatively large value of $k_{apd,b} = 4.0 \times 10^{-4}$m/s was assumed to ensure efficient capturing of shear-activated platelets to the bio-surfaces (by the vWF-GP1b complex). The introduction of the vWF amplification function, $\boldsymbol{f}_{vWF}$, results in three new parameters, $C_{vWF}$, $\tau_{1/2}$ and $\Delta\tau$, that must be determined. We found that $C_{vWF} = 4.0 \times 10^3$, $\tau_{1/2\,=\,160}\ Pa$ and $\Delta\tau = 15 Pa$ provided the best agreement with the experiments by Tovar-Lopez et al. (2010) (Tovar-Lopez et al., 2010). The remaining parameters are the same as those published in Wu et al. (2017) (Wu et al., 2017).

Figure 5 (a) and Figure 5 (b) show the platelets deposition in the x-y plane at the z-position of $30\mu m$ for the expansion angle of $\theta = 60°$ observed in the experiments (Tovar-Lopez et al., 2010) and predicted by our numerical model. It can be seen that the simulations and the experiments demonstrate excellent agreement both temporally and spatially. It should be noted that to account for the finite depth-of-field of the experimental images, the numerical results shown in Figure 5 (b) are averaged in the z-direction assuming a $10\mu m$ depth of field (Wu, Yang, Antaki, Aubry, & Massoudi, 2015; Zhao et al., 2008). As seen in the figure, all depositions took place in the expansion region downstream of the stenosis and there is no observable deposition in the stenosis gap. Figure 5 (c) shows the 3D rendering of the simulated thrombus. At 60s the thrombus is largest in the mid-plane of the channel (z=65$\mu m$). As time progresses, the thrombus becomes both longer and thicker. Figure 5 (d) demonstrates that the growing thrombus distorts the streamlines in the channel, potentially exacerbating the deposition of platelets. To investigate the relative role of vWF, additional simulations were performed in which $\boldsymbol{f}_{vWF} = 0$. In all cases studied *no platelets deposition* occurred. This is in agreement with the experimental observations by Tovar-Lopez et al. (2010) (Tovar-Lopez et al., 2010).

Additional simulations were performed to investigate the effect of the expansion angle $\theta$ on the deposition patterns. All other parameters remained the same as in the previous case. Figure 6 compares the numerically predicted and experimentally measured volume fraction of deposited platelets for $\theta = 30°$. Compared to the case $\theta = 60°$ (Figure 4), both experiments and numerical simulations predicted a dramatic reduction of platelet deposition, and dramatically reduced accumulation over time (from 60 to 360s). Figure 6 (b) provides simulation results for an intermediate angle of $\theta = 40°$ in which the amount of deposition is slightly greater than $\theta = 60°$ yet still much less than the case for $\theta = 30°$.This observation is quantified in Figure 6 (c), which illustrates a nonlinear relationship between expansion angle and deposition rate. It also suggests the existence of a critical angle (between $\theta = 40°$ and 60°) that delimits conditions for a stable versus growing thrombus.

Figure 7 shows the distribution of the shear rate, shear stress accumulation and platelets activation with different expansion angles. Although the magnitude of the peak shear rate is similar for all angles, the shear accumulation clearly increases with steeper (increasing) expansion angle. It is also noteworthy that while the shear field is symmetric about the apex of the stenosis, the shear accumulation grows in the downstream direction. The platelet activation function field, Figure 7 (c), is congruent with the shear accumulation field.

### Effects of flow rate (Reynolds number), stenosis height and vWF activity

In the simulations above, it was established that the distribution of the shear stress around the stenosis determines the platelets deposition. In this section, we further study two factors related to the shear stress distribution: the flow rate (Reynolds number) and stenosis gap size, $L_c$. All other parameters are the same as the previous studies. The effect of Reynolds number is illustrated in Figure 8, which provides the baseline case (Re = 0.70) shown in Figure 4, as well as 25% greater and lower (0.88 and 0.53, respectively.) Despite the relatively small perturbation in this parameter, the Re=0.88 case produces a significantly larger thrombus, while Re=0.53 yields almost negligible amount of deposition. The corresponding velocity fields are presented in Figure 8 (c). Figure 8 (d) illustrates the mechanism for continued growth of the thrombus, namely the increasing concentration of activated platelets that are shed downstream of the stenosis into the layer adjacent to the deposited platelets. The activation of platelets, in turn, can be attributed to the elevated shear rate in the stenosis, Figure 8 (e), resulting in the enhanced shear stress accumulation (shear activation) shown in Figure 8 (f). For the case of Re = 0.88, elevated shear accumulation can also be observed along the upper wall. Figure 8 (g) provides a quantitation of platelet deposition versus time for the three cases and suggests a critical value (between Re=0.53 and 0.70) below which the amount of deposition quickly stabilizes and shows no further growth.

Figure 9 illustrates the effect of the stenosis gap size, $L_c$, hence the degree of stenosis. Figure 9 (a) and (b) show a direct relationship between the gap size and deposition: $L_c = 22.5\mu m$ (77.5% stenosis) produces less deposition compared to the baseline, $L_c = 20\mu m$ (80% stenosis); and $L_c = 17.5\mu m$ (82.5% stenosis) produces more deposition. Interestingly, there is a noticeable, albeit small, degree of deposition at the apex of the stenosis for $L_c = 22.5\mu m$. This can be attributed to the relatively lower shear washing in the larger-gap stenosis. For the greatest degree of stenosis, $L_c = 17.5\mu m$, thrombus deposition can be observed on the upper wall. For the straight channel without stenosis (not shown), no thrombus is observed. The effect of decreasing $L_c$ is similar to that of increasing $Re$, since both increase the shear rate (thus the shear stress accumulation and platelet activation) in the neighborhood of the stenosis region, as shown in Figure 9 (f), (g) and (h). These results are depicted quantitatively as a function of time in Figure 10 (a).

To assess the influence of vWF on the shear-mediated thrombosis, the baseline case was repeated with increased vWF activity, as well as with vWF eliminated completely. Here, the vWF activity implicitly represents the combined effect of vWF and its adhesion receptors, such as GPIB and αIIbβ3. This was achieved by scaling the enhancement coefficient, $C_{vWF}$. Figure 10 (b) indicates that increasing vWF activity amplifies the rate of platelets deposition dramatically. Conversely, completely inhibiting vWF (which could also represent the inhibition of vWF receptors) results in negligible platelet deposition; this corresponds to the experimental observation by Tovar-Lopez et al. (2010) (Tovar-Lopez et al., 2010) as well.

## 4. Discussion

Because of the supra-physiological levels of shear occurring in these devices, we found it necessary to supplement our previously reported thrombosis model to account for the essential role of vWF in high-shear thrombosis. Our revised model incorporates mechanisms identified by experimental studies of vWF-mediated thrombosis in stenosed vessels and microfluidic channels, and aims to replicate these experimental observations (Nesbitt et al., 2009; Tovar-Lopez et al., 2010; Westein et al., 2013). A key assumption of our model is that, in regions of the flow field in which shear is sufficiently elevated, surface- and membrane-bound vWF will unfold, causing flowing platelets to be captured, and tethered, whereupon they can be activated by prolonged exposure to shear. This assumption is supported by a recent report by Diamond (2016) who directly observed platelets arrested on the surface of the VWF fibers that were entrained downstream from a micropost within a microfluidic channel (Diamond, 2016). He further observed platelet activation (by P-selectin) when shear rates exceeded 3000 s−1. This value is comparable to the threshold ($\tau_c$) in our platelet-shear accumulation model (Equation 2).

The simulations reported here predicted patterns of deposition downstream of the stenosis in the absence of biochemical agonists – consistent with the experimental observations of Lkeda et al. (1991) (Ikeda et al., 1991) and microfluidic experiments of Nesbitt et al. (2009) (Tovar-Lopez et al., 2010). This phenomenon is the result of competing effects of between shear activation and shear washing. Blood entering the stenosis experiences the greatest level of shear at its apex, causing adsorbed vWF to unfold, capturing flowing platelets and exposing them to prolonged shear stress and inducing a conformational change, i.e. causing them to become activated (see Figure 7). Due to the decreasing level of shear in the expansion zone downstream of the stenosis, activated platelets are able to form stable aggregates. The simulations also found that the quantity of deposition increased with increasing degree of stenosis, which was also observed independently by both Nesbitt et al. (2009) (Tovar-Lopez et al., 2010) and Westein et al. (2013) (Westein et al., 2013). The simulations also demonstrated a direct relationship between deposition rate and vWF activity. When vWF was eliminated, negligible platelets deposition was observed (See Figure 10 (b)). This is corroborated by the cone-plate studies by Peterson et al. (1987) who found that, in the absence of vWF or GPIb, shear-induced platelet aggregation was inhibited (Peterson et al., 1987). In addition to von Willebrand disease (VWD), this result is also relevant to acquired vWF syndrome believed to be responsible for bleeding episodes in patients with continuous flow ventricular assist devices (cfVADs) (Akhter, 2016; Kang et al., 2016; Muthiah et al., 2016; Netuka et al., 2016).

The overall approach adopted by our model treats whole blood as a continuum - as contrasted with previous meso-scale simulations that considers interaction between individual cells (Flamm et al., 2012; Xu et al., 2010). The advantage is to enable macro-scale simulations which otherwise would be computationally prohibitive -- especially in consideration of many unknown parameters. A disadvantage of a continuum approach is the inability to simulate the stochastic phenomena of embolization, for example, manifested experimentally in Tovar-Lopez et al. (2010) (Tovar-Lopez et al., 2010) by large fluctuations in aggregate size versus time. Instead, the simulated deposition increases smoothly, and

monotonically. Nevertheless, the simulation results are consistent with the trend line of the experimental aggregation traces. Furthermore, in our model there are a few parameters, related to the materials (such as viscosity), the flow (such as the drag coefficient), the species activities (such as vWF unfolding). In general, some of these parameters can be estimated from the existing experimental data, and sometimes in the absence of such data, it is necessary to either estimate or approximate them using other methods such as the time evolution of the shape of the thrombus.

In this study, the role of vWF was *implicitly* modelled as an enhancement function for shear stress accumulation, based on an experimentally observed relationship between shear and vWF unfolding, reported by Lippok et al. (2016) (Lippok et al., 2016) and Schneider et al. (2007) (Schneider et al., 2007). Consequently, this function does not *explicitly* account the multimer concentration, unfolding, and adsorption. Likewise, the present model overlooks the mechanism of the self-association of vWF into massive fibers – as reported recently by Diamond (2016) (Diamond, 2016). In addition, the current model is not sensitive to the elongational flow gradients which seem to play an important role in vWF unfolding as demonstrated by Westein et al. (2013) (Westein et al., 2013). Future development of our model will include transport and adsorption of vWF species and direct interaction with the platelets. Likewise, the model does not explicitly consider downstream migration of platelets initially captured by vWF into to the expansion region, for example due to the short half-life of vWF-GPIb bonds (Savage & Ruggeri, 2007). Instead, this phenomenon is represented in the rate constant for shear activation $k_{spac}$ which is related to the time constant for morphological change of platelets exposed to shear. We also acknowledge that these simulations were focused exclusively on two experimental studies in micro-channel stenoses in which bio-chemical agonists were inhibited. This allowed us to focus solely on the role of shear activation and vWF, although at the expense of overlooking the synergistic effects of other factors and feedback mechanisms. Therefore extension of this work will consider experiments without agonists blockage *in vivo* and *in vitro* (Colace & Diamond, 2013; Diamond, 2016; Westein et al., 2013).

## 5. Conclusions

In this paper, we investigated a new mathematical model for vWF-mediated thrombus formation in an idealized stenosis. This model was built upon a previous model that considered blood as a multi-constituent mixture comprised of a linear fluid component and a thrombus (solid) component; the chemical and the biological species related to the thrombosis are modeled by a system of coupled convection-reaction-diffusion (CRD) equations. The activation of the platelets by shear was assumed to depend on their shear stress accumulation (history), and the role of vWF was represented by an enhancement function on the shear stress accumulation depending on its sheardependent degree of unfolding. Computational simulations using this model accurately replicated the experimentally observed formation of vWF-mediated thrombus in a stenosis: temporally and spatially. Both experiments and simulations indicated patterns of platelet deposition downstream of the stenosis that is reduced with a smaller expansion angle, increased with greater degree of stenosis and directly related to the level of vWF activity. It is hoped that the model described here may contribute to deeper quantitative understanding of vWF-

mediated thrombosis, and to the development of more hemo-compatible devices in the future.

## Supplementary Material

Refer to Web version on PubMed Central for supplementary material.

## Acknowledgement

This work was jointly supported by Natural Science Foundation of China (11802135) and NIH grant 1 R01 HL089456.

## Appendix A.: Expanded governing questions of chemical/biological species

Provided below are the full set of governing equations in expanded form.

## Unactivated resting PLTs in flow ([RP])

$$\frac{\partial[RP]}{\partial t} + div(\boldsymbol{v}[RP]) = div(D_P \nabla[RP]) - k_{apa}[RP] - k_{spa}[RP] - k_{rpd}[RP] \quad \text{(A1)}$$

where $\boldsymbol{v}$ is the velocity of the fluid (blood), $D_P$ is the diffusivity of the platelets, $k_{apa}$ and $k_{spa}$ are the platelets activation rate due to agonists and shear stress, and $k_{rpd}$ is the deposition rate between [RP] and deposited platelets. The detail definition of the $k_{rpd}$ in mathematical and numerical see Appendix 2.

## Activated platelets in flow ([AP])

$$\frac{\partial[AP]}{\partial t} + div(\boldsymbol{v}[AP]) = div(D_P \nabla[AP]) + k_{apa}[RP] + k_{spa}[RP] - k_{apd}[AP] \quad \text{(A2)}$$

where $k_{apa}$ is the deposition rate between [AP] and deposited platelets. The detail definition of the $k_{apa}$ in mathematical and numerical see Appendix 2.

## Deposited resting platelets ([$RP_d$])

$$\frac{\partial[RP_d]}{\partial t} = (1-\theta)k_{rpd}[RP] - k_{apa}[RP_d] - k_{spa}[RP_d] - f_{emb}[RP_d] \quad \text{(A3)}$$

where $(1-\theta)k_{rpd}[RP]$ is the percentage of $[RP]$ activated by contact with biomaterial surfaces and formatted thrombus, $f_{emb}$ is the cleaning rate of deposited platelets due to shear stress.

## Deposited activated platelets ([$AP_d$])

$$\frac{\partial[AP_d]}{\partial t} = \theta k_{rpd}[RP] + k_{apd}[AP] + k_{apa}[RP_d] + k_{spa}[RP_d] - (f_{emb} + f_{stb})[AP_d] \tag{A4}$$

where $f_{stb}$ is the stabilization rate parameter of [$AP_d$], which convert deposited thrombus to be stabilized thrombus which is harder to be cleaned by shear stress.

## Deposited and stabilized platelets ([$AP_s$])

$$\frac{\partial[AP_s]}{\partial t} = f_{stb}[AP_d] \tag{A5}$$

## PLT-released agonists (ADP) ([$a_{pr}$])

$$\frac{\partial[a_{pr}]}{\partial t} + div(\boldsymbol{v}[a_{pr}]) = div(D_{apr}\nabla[a_{pr}]) + \lambda_j (k_{apa}[RP] + k_{spa}[RP] + k_{apa}[RP_d] + k_{spa}[RP_d] + \theta k_{rpd}[RP]) - k_{1,j}[a_{pr}] \tag{A6}$$

where $\lambda_j$ is the amount of agonist $j$ released per platelet and $k_{1,j}$ is the inhibition rate constant of agonist $j$; and $j$ represents ADP for current specie. Therefore $\lambda_j k_{apa}[RP]$ and $\lambda_j k_{apa}[RP_d]$ are the ADP releasing attributed to the activation of unactivated platelets due to agonist, $\lambda_j k_{spa}[RP]$ and $\lambda_j k_{spa}[RP_d]$ are the ADP releasing attributed to the activation of unactivated platelets due to shear stress and $\lambda_j \theta k_{rpd}[RP]$ represents the ADP releasing attributed to the platelets activation due to contact. $k_{1,j}[a_{pr}]$ is the inhibition rate of ADP.

## PLT-synthesized agonists ($TxA_2$) ([$a_{ps}$])

$$\frac{\partial[a_{ps}]}{\partial t} + div(\boldsymbol{v}[a_{ps}]) = div(D_{aps}\nabla[a_{ps}]) + s_{pj}([AP] + [AP_d]) - k_{1,j}[a_{ps}] \tag{A7}$$

where $s_{pj}$ is the rate constant of synthesis of the agonist $j$; and $j$ represents $TxA_2$ for current specie. Therefore $s_{pj}[AP]$ and $s_{pj}[AP_d]$ represent the rate of synthesis of $TxA_2$ due to activated platelets in flow and deposited activated platelets. $k_{1,j}[a_{ps}]$ is the inhibition rate of $TxA_2$.

## Prothrombin ([PT])

$$\frac{\partial[PT]}{\partial t} + div(\boldsymbol{v}[PT]) = div(D_{PT}\nabla[PT]) - \varepsilon[PT](\phi_{at}([AP] + [AP_d]) + \phi_{rt}([RP] + [RP_d])) \tag{A8}$$

where $\varepsilon$ is the unit conversion which is from NIH units to SI units, $\phi_{at}$ and $\phi_{rt}$ are the thrombin generation rate constant on the surface of activated platelets and unactivated resting platelets. Therefore $\phi_{at}[AP]$ and $\phi_{rt}[RP]$ are the thrombin generation rate due to activated and resting platelets in flow, while $\phi_{at}[AP_d]$ and $\phi_{rt}[RP_d]$ are the thrombin generation rate due to deposited activated and unactivated platelets.

## Thrombin ([TB])

$$\frac{\partial[TB]}{\partial t} + div(\boldsymbol{v}[TB]) = div(D_{TB}\nabla[TB]) + [\mathrm{PT}](\phi_{at}([AP] + [AP_d]) + \phi_{rt}([RP] + [RP_d])) - \Gamma[TB] \tag{A9}$$

where Γ is the Griffith's template model for the kinetics of the heparin-catalyzed inactivation of thrombin by ATIII. Therefore $\Gamma[TB]$ is the inactivation rate of thrombin by ATIII.

## ATIII ([AT])

$$\frac{\partial[AT]}{\partial t} + div(\boldsymbol{v}[AT]) = div(D_{AT}\nabla[AT]) - \Gamma\varepsilon[TB] \tag{A10}$$

where $\Gamma\varepsilon[TB]$ is the consumption rate of ATIII due to inactivation of thrombin.

## Appendix B.: Variables, coefficients and parameters of the thrombosis model

**Table A1.**

Source terms associated with platelets. See Figure 1 for definition of reaction rates, k.

| Species | $[C_i]$ abbreviation | $S_i$ form |
|---|---|---|
| Unactivated Resting PLTs | [RP] | $-k_{apa}[RP] - k_{spa}[RP] - k_{rpd}[RP]$ |
| Activated PLTs | [AP] | $-k_{apa}[RP] - k_{spa}[RP] - k_{apd}[RP]$ |
| Deposited Resting PLTs | $[\mathrm{RP_d}]$ | $(1-\theta)\,k_{rpd}[RP] - k_{apa}[RP_d] - k_{spa}[RP_d] - f_{emb}[RP_d]$ |
| Deposited Activated PLTs | $[\mathrm{AP_d}]$ | $\theta k_{rpd}[RP] + k_{apd}[AP] + k_{apd}[RP_d] + k_{spa}[RP_d] - (f_{emb} + f_{stb})[AP_d]$ |
| Deposited and stabilized PLTs | $[\mathrm{AP_s}]$ | $f_{stb}[AP_d]$ |

**Table A2.**

Source terms for chemical species of the model.

| Species | $[C_i]$ abbreviation | $S_i$ form |
|---|---|---|
| PLT-released agonists (ADP) | $[\mathrm{a_{pr}}]$ | $\lambda_f(k_{apa}[RP] + k_{spa}[RP] + k_{apa}[RP_d] + k_{spa}[RP_d] + \theta k_{rpd}[RP]) - k_{1,j}[\mathrm{a_{pr}}]$ |
| PLT-synthesized agonists ($TxA_2$) | $[\mathrm{a_{ps}}]$ | $s_{pj}([AP] + [AP_d] - k_{1,j}[\mathrm{a_{ps}}]$ |
| Prothrombin | [PT] | $-\varepsilon[\mathrm{PT}](\phi_{at}([AP] + [AP_d]) + \phi_{rt}([RP] + [AP_d]))$ |

| Species | $[C_i]$ abbreviation | $S_i$ form |
|---|---|---|
| Thrombin | [TB] | $-\Gamma \cdot [TB] + [PT]\,(\phi_{at}([AP] + [AP_d]) + (\phi_{at}([RP] + [RP_d]))$ |
| ATIII | [AT] | $-\Gamma e\,[TB]$ |

**Table A3.**

Species units, coefficient of species diffusion and initial condition. $\gamma$ is the local shear rate. For more detail see Sorenson(Sorensen et al., 1999a, 1999b) and Goodman (Goodman et al., 2005).

| Species | Species units | $D_i$ $(m^2 s^{-1})$ | Initial (inlet) condition in blood |
|---|---|---|---|
| [RP] | PLT $m^{-3}$ | $1.58 \times 10^{-13} + 6.0 \times 10^{-13}\gamma$ | $1.5 \times 10^{14} - 3.0 \times 10^{14}$(Human)<br>$1.9 \times 10^{14} - 10.0 \times 10^{14}$(Mouse) |
| [AP] | PLT $m^{-3}$ | $1.58 \times 10^{-13} + 6.0 \times 10^{-13}\gamma$ | 0.01[RP] − 0.05[RP] |
| [$a_{pr}$] | nmol $m^{-3}$ | $2.57 \times 10^{-10}$ | 0.0 |
| [$a_{ps}$] | nmol $m^{-3}$ | $2.14 \times 10^{-10}$ | 0.0 |
| [PT] | nmol $m^{-3}$ | $3.32 \times 10^{-11}$ | $1.1 \times 10^{6}$ |
| [TB] | $Um^{-3}$ | $4.16 \times 10^{-11}$ | 0.0 |
| [AT] | nmol $m^{-3}$ | $3.49 \times 10^{-11}$ | $2.844 \times 10^{6}$ |
| [$RP_d$] | PLT $m^{-3}$ | N/A | 0.0 |
| [$AP_d$] | PLT $m^{-3}$ | N/A | 0.0 |
| [$AP_s$] | PLT $m^{-3}$ | N/A | 0.0 |

**Table A4(a).**

Boundary conditions..

| Species $[C_i]$ | $j_i$ form | Description |
|---|---|---|
| [RP] | $-Sk_{rpdb}[RP]$ | Consu mption due to [RP]-surface adhesion; Generation due to shear embolization. |
| [AP] | $-Sk_{apdb}[AP]$ | Consumption due to [AP]-surface adhesion; Generation due to shear embolization. |
| [$a_{pr}$] | $\lambda_j(k_{apa}[RP_d] + k_{spa}[RP_d] + \theta Sk_{rpdb}[RP])$ | Generation due to agonists and shear activation of [$RP_d$]; Generation due to surface contact activation of [RP]-surface adhesion. |
| [$a_{ps}$] | $S_{pj}[AP_d]$ | Platelet-synthesized generation due to [$AP_d$] |
| [PT] | $-e$ [PT] $(\phi_{at}[AP_d] + \phi_{rt}[RP_d])$ | Consumption due to thrombin, [TB], generation. |
| [TB] | [PT] $(\phi_{at}[AP_d] + \phi_{at}[RP_d])$ | Generation from prothrombin [PT] due to deposited platelets. |
| [AT] | 0.0 | No reaction flux. |

**Table A4(b).**

Species boundary conditions. (See Table A5 definitions of each of the terms.)

| Species $[C_i]$ | $j_i$ form | Description |
|---|---|---|
| $[RP_d]$ | $\int_0^t (1-\theta) S k_{rpdb}\,[RP] - k_{apa}[RP_d] - k_{spa}[RP_d] - f_{embb}[RP_d]dt$ | Generation due to [RP]-surface adhesion; Consumption due to agonists and shear activation; Consumption due to shear embolization. |
| $[AP_d]$ | $\int_0^t S k_{apdb}[AP] + \theta S k_{rpdb}[RP] + k_{apa}[RP_d] + k_{spa}[RP_d] - (f_{embb} + f_{stb})[AP_d]dt$ | Generation due to [AP]-Surface adhesion; Generation due to surface contact activation of [RP]-Surface adhesion; Generation due to agonists and shear activation of [RP]; Consumption due to shear embolization and stabilization. |
| $[AP_s]$ | $\int_0^t f_{stb}[AP_d]dt$ | Generation due to stabilization. |

**Table A5.**

Value or expression and description of reaction terms and parameters of the model.

| Terms | Value or expression | units | Description |
|---|---|---|---|
| $k_{apa}$ | $\begin{cases} 0, \Omega < 1.0 \\ \frac{\Omega}{t_{ct}}, \Omega \geq 1.0 \\ \frac{1}{t_{act}}, \frac{\Omega}{t_{ct}} \geq \frac{1}{t_{act}} \end{cases}$ | $(s^{-1})$ | Platelets activation due to agonists; $t_{ct}$ is the characteristic time, which can be used for adjusting the activation rate, and here we choose $t_{ct} = 1s$ as provided Sorensen (Sorensen et al., 1999a, 1999b); $\left(k_{apa} = \frac{1}{t_{act}}, \frac{\Omega}{t_{ct}} \geq \frac{1}{t_{act}}\right)$ implies the reaction cannot be faster than platelets physical activation procedure and 99% platelets will be activated during the activation procedure if the agonists or shear stress is large enough. $t_{act}$ is the characteristic time; $t_{act}$ is suggested to range from 0.1s to 0.5s considering the results by Frojmovic et. al (Frojmovic, Mooney, |

| Terms | Value or expression | units | Description |
|---|---|---|---|
| | | | & Wong, 1994) and Richardson (Richardson, 1973). |
| Ω | $\sum_{j=1}^{n_a} w_j \frac{a_j}{a_{j,crit}}$ | (N/A) | $a_j$ refers to the concentration of ADP, $TxA_2$ and Thrombin. Value of $w_j$ and $a_{j,crit}$ see Table A6. |
| $k_{spa}$ | $k_{spac} H(SA - SA_c)$ | ($s^{-1}$) | Platelets activation due to shear accumulation. The definition of $H(SA - SA_c)$, see main text. |
| $k_{spac}$ | 100 | ($s^{-1}$) | This term is derived from considering the time constant for morphological change of platelets exposed to shear. |
| $f_{sa}$ | $\frac{1}{t_e} H(\tau - \tau_c)$ | ($s^{-1}$) | Rate function of the platelet stress accumulation. The definition of $H(\tau - \tau_c)$, see main text. |
| $t_e$ | $10^{\left(-2 * log_{10}^{\tau/\tau_r} + 5.6758\right)} \cdot s$ | ($s$) | Exposure time needed for platelet activation under certain shear stress. Here $\tau$ has the unites of $dynes/cm^2$. |
| $f_{vWF}$ | $\frac{C_{vWF}}{1 + exp(-(\tau - \tau_{1/2})/\Delta\tau)}$ | (N/A) | The *amplification function* due to the capture of platelet by vWF. |
| $C_{vWF}$ | $3 \times 10^3$ | (N/A) | The maximum achievable value of the enhancement constant |
| $\tau_{1/2}$ | 160 | (Pa) | Whear stress at which half of the vWF monomers are fully unfolded |
| $\Delta\tau$ | 15 | (Pa) | The duration of the transition |
| $k_{rpd}$ | $div\left(k_{pd,f}\vec{n}\right)k_{ra}$ | ($s^{-1}$) | Unactivated platelets - deposited activated platelets ([RP]-[$AP_d$]), deposition rate. $f$ refers to the face of a mesh cell and $\vec{n}$ is the unit normal to the face. Details about how this term is calculated are provided in Appendix C. |
| $k_{ra}$ | $3.0 \times 10^{-6}$ | (m $s^{-1}$) | Constant related to $k_{rpd}$, see (Sorensen et al., 1999a, 1999b). |
| $k_{apd}$ | $div\left(k_{pd,f}\vec{n}\right)k_{aa}$ | ($s^{-1}$) | Activated platelets-deposited activated platelets ([AP]-[$AP_d$]) deposition rate. Details about how this term is calculated are provided in Appendix C. |
| $k_{aa}$ | $3.0 \times 10^{-5}$ | (m $s^{-1}$) | Constant related to $k_{apd}$, see (Sorensen et al., 1999a, 1999b). |
| $f_{emb}$ | $\mathscr{D}_{PLT} div\left(k_{emb,f}\vec{n}\right)\left(1 - exp\left(-0.0095\frac{\tau}{\tau_{emb}}\right)\right)$ | $s^{-1}$ | Platelet embolization due to shear stress; Expression $exp(-0.0095\tau)$ was suggested by Goodman(Goodman et al., 2005). $\mathscr{D}_{PLT} = 2.78 \times 10^{-6} m$ is the hydraulic diameter of platelets. |
| $k_{emb,f}$ | $k_{emb,f} = \begin{cases} 1, k_{pd,f} > 0 \\ 0, k_{pd,f} = 0 \end{cases}$ | $s^{-1}$ | |
| $\tau_{emb}$ | 120 | $\frac{dyne}{cm^{-2}}$ | Platelet shear embolization related constant.(Goodman et al., 2005) |
| $f_{embb}$ | $\left(1 - exp\left(-0.0095\frac{\tau}{\tau_{embb}}\right)\right)$ | $s^{-1}$ | Platelet embolization in boundary due to shear stress. |
| $\tau_{emb,b}$ | To be determined, depends on bio-materials. | $\frac{dyne}{cm^{-2}}$ | Platelet shear embolization related constant. |

| Terms | Value or expression | units | Description |
|---|---|---|---|
| $PLT_{max}$ | $\frac{PLT_{s,\max}}{\mathscr{D}_{PLT}}$ | PLT $m^{-3}$ | The maximum concentration of platelets in space. $PLT_{s,max} = 7 \times 10^{10}\ PLTm^{-2}$ is the total capacity of the surface for platelets; $\mathscr{D}_{PLT} = 2.78 \times 10^{-6} m$. |
| $\lambda_j$ | $2.4 \times 10^{-8}$ | nmol $PLT^{-3}$ | The amount of agonist $j$ released per platelet. |
| $\theta$ | 1.0 | (N/A) | Platelets activation by contact. |
| $k_{1,j}$ | $\begin{cases} 0.0161 \text{ for TxA2} \\ 0.0 \text{ for ADP} \end{cases}$ | ($s^{-1}$) | The inhibition rate constant of agonist. |
| $s_{pj}$ | $\begin{cases} 9.5 \times 10^{-12} \text{ for TxA2} \\ 0.0 \text{ for ADP} \end{cases}$ | nmol $PLT^{-3}$ | The rate constant of synthesis of an agonist. |
| $\varepsilon$ | $9.11 \times 10^{-3}$ | nmol $U^{-1}$ | Unit conversion. From NIH units to SI units. |
| $\phi_{at}$ | $3.69 \times 10^{-15}$ | $m^3$ $nmol^{-1}$ $PLT^{-1}$ $U\ s^{-1}$ | Thrombin generation rate on the surface of activated platelets |
| $\phi_{rt}$ | $6.5 \times 10^{-16}$ | $m^3$ $nmol^{-1}$ $PLT^{-1}$ $U\ s^{-1}$ | Thrombin generation rate on the surface of unactivated platelets |
| $\Gamma$ | $\frac{k_{1,T}[H][AT]}{\alpha K_{AT} K_T + \alpha K_{AT} \varepsilon[TB] + [AT]\varepsilon[TB]}$ | ($s^{-1}$) | Griffith's template model for the kinetics of the heparin-catalyzed inactivation of thrombin by ATIII. |
| $k_{1,T}$ | 13.333 | ($s^{-1}$) | A first-order rate constant. |
| $[H]$ | $0.1 \times 10^6$ | nmol $m^{-3}$ | Heparin concentration, assuming specific activity of 300 U $mg^{-1}$ and molecular weight of 16 kDa. (Engelberg & Dudley, 1961; Sorensen et al., 1999b) |
| $\alpha$ | 1.0 | (N/A) | A factor to simulate a change in affinity of heparin for ATIII when it is bound to thrombin or for thrombin when it is bound to ATIII. |
| $K_{AT}$ | $0.1 \times 10^6$ | nmol $m^{-3}$ | The dissociation constant for heparin/ATIII. |
| $K_T$ | 3.50 × 104 | nmol $m^{-3}$ | The dissociation constant for heparin/thrombin. |
| $S$ | $1 - \frac{[RP_{db}] + [AP_{db}] + [AP_{sb}]}{PLT_{s,max}}$ | (N/A) | Percentage of the wall (boundary) not been occupied by deposited platelets. |
| $k_{rpd,b}$ | To be determined, depends on bio-materials. | (m $s^{-1}$) | Unactivated platelet-boundary(wall) deposition rate. |
| $k_{apd,b}$ | To be determined, depends on bio-materials. | (m $s^{-1}$) | Activated platelet-boundary(wall) deposition rate. |
| $f_{stb}$ | 0.0 | ($s^{-1}$) | Deposited activated platelet stabilization rate. |
| $\Phi 0$ | $\frac{RP_d + AP_d + AP_s}{PLT_{max}}$ | (N/A) | Volume fraction of deposited platelets |

**Table A6.**

Threshold concentration of that agonist for platelet activation and agonist-specific weight (Goodman et al., 2005; Sorensen et al., 1999a, 1999b; Wu et al., 2017). It should be noticed that the threshold of the agonist may vary for some certain according to different experimental studies.

| Species | $a_{j,crit}$ | $w_j$ |
|---|---|---|
| ADP($[a_{pr}]$) | $1.00 \times 10^6$nmol $m^{-3}$ | 1 |
| $TxA_2$($[a_{ps}]$) | $0.20 \times 10^6$nmol $m^{-3}$ | 3.3 |
| Thrombin([TB]) | $0.1 \times 10^6$U$m^{-3}$ | 30 |

## Appendix C.: Mathematical and Numerical Considerations for Deposition Rates krpd and kapd

Provided below are mathematical and numerical considerations about the two terms in equations of platelet deposition, that represent the rate of deposition to the surface of the thrombus by unactivated resting platelets ($k_{rpd}$) and activated platelets ($k_{apd}$) in the free stream. Referring to the finite volume schematic depicted in Figure S1, the $k_{rpd}$ of the finite-volume-cell 5 is calculated as

$$k_{rpd} = div\left(k_{pd,f}\vec{\boldsymbol{n}}\right)k_{ra} \tag{A11}$$

where $k_{ra}$ is a constant, $\vec{\boldsymbol{n}}$ is the normal to the finite-volume-face, and $f$ refers to the faces shared by adjacent cells 2, 4, 6 and 8. Assuming that thrombus tends to grow layer by layer, when the volume fraction of the deposited platelets of a finite-volume cell $\phi$ is greater than a critical value $\phi_c$ (for example, 0.74, which is the maximum packing fraction for spheres), this cell is able to influence the neighbor cells. Therefore

$$k_{pd,f} = \begin{cases} \dfrac{[AP_d]_f}{PLT_{\max}}, \phi > \phi_c \\ 0, \phi < \phi_c \end{cases} \tag{A12}$$

where $\frac{[AP_d]_f}{PLT_{\max}}$ represents the percentage of the area occupied by deposited activated platelets at that mesh face. This rule does not apply to the boundary faces.

## References

Akhter SA (2016). Continuous-flow left ventricular assist devices and bleeding events: Is there a biological role for decreasing pump speed? The Journal of Thoracic and Cardiovascular Surgery, 151(6), 1755–1756. [PubMed: 26971386]

Anand M, Rajagopal K, & Rajagopal KR (2005). A model for the formation and lysis of blood clots. Pathophysiology of Haemostasis and Thrombosis, 34(2–3), 109–120. [PubMed: 16432312]

Anand M, Rajagopal K, & Rajagopal KR (2003). A model incorporating some of the mechanical and biochemical factors underlying clot formation and dissolution in flowing blood: review article. Journal of Theoretical Medicine, 5(3–4), 183–218.

Anand M, Rajagopal K, & Rajagopal KR (2008). A model for the formation, growth, and lysis of clots in quiescent plasma. A comparison between the effects of antithrombin III deficiency and protein C deficiency. Journal of Theoretical Biology, 253(4), 725–738. [PubMed: 18539301]

Anand Mohan, & Rajagopal KR (2002). A mathematical model to describe the change in the constitutive character of blood due to platelet activation. Comptes Rendus Mécanique, 330(8), 557–562.

Anand Mohan, & Rajagopal KR (2017). A short review of advances in the modelling of blood rheology and clot formation. Fluids, 2(3), 35.

Anderson GH, Hellums JD, Moake J, & Alfrey CP (1978). Platelet response to shear stress: changes in serotonin uptake, serotonin release, and ADP induced aggregation. Thrombosis Research, 13(6), 1039–1047. [PubMed: 749261]

Anderson GH, Hellums JD, Moake JL, & Alfrey CP Jr (1977). Platelet lysis and aggregation in shear fields. Blood Cells, 4(3), 499–511.

Ataullakhanov FI, & Panteleev MA (2005). Mathematical modeling and computer simulation in blood coagulation. Pathophysiology of Haemostasis and Thrombosis, 34(2–3), 60–70. [PubMed: 16432308]

Bodnár T (2014). On the Eulerian formulation of a stress induced platelet activation function. Mathematical Biosciences, 257, 91–95. [PubMed: 24976251]

Brown CH III, Lemuth RF, Hellums JD, Leverett LB, & Alfrey CP (1975). RESPONSE OF HUMAN PLATELETS TO SHEAR STRESS. ASAIO Journal, 21(1), 35–39.

Cannegieter SC, Rosendaal FR, & Briët E (1994). Thromboembolic and bleeding complications in patients with mechanical heart valve prostheses. Circulation, 89(2), 635–641. from http://circ.ahajournals.org/content/89/2/635.short [PubMed: 8313552]

Colace TV, & Diamond SL (2013). Direct observation of von Willebrand factor elongation and fiber formation on collagen during acute whole blood exposure to pathological flow. Arteriosclerosis, Thrombosis, and Vascular Biology, 33(1), 105–113.

Colantuoni G, Heliums JD, Moake JL, & Alfrey CP Jr (1977). The response of human platelets to shear stress at short exposure times. ASAIO Journal, 23(1), 626–630.

Combariza ME, Yu X, Nesbitt WS, Mitchell A, & Tovar-Lopez FJ (2015). Nonlinear dynamic modelling of platelet aggregation via microfluidic devices. IEEE Transactions on Biomedical Engineering, 62(7), 1718–1727. [PubMed: 25706500]

Diamond SL (2016). Flow and delta-P dictate where thrombin, fibrin, and von Willebrand Factor will be found. Thrombosis Research, 141, S22–S24. [PubMed: 27207416]

Engelberg H, & Dudley A (1961). Plasma heparin levels in normal man. Circulation, 23(4), 578–581. [PubMed: 13696820]

Fauci AS (1998). Harrison's principles of internal medicine (Vol. 2). Mcgraw-hill New York.

Flamm MH, Colace TV, Chatterjee MS, Jing H, Zhou S, Jaeger D, … Diamond SL (2012). Multiscale prediction of patient-specific platelet function under flow. Blood, 120(1), 190–198. [PubMed: 22517902]

Fogelson AL (1984). A mathematical model and numerical method for studying platelet adhesion and aggregation during blood clotting. Journal of Computational Physics, 56(1), 111–134.

Fogelson AL, & Neeves KB (2015). Fluid mechanics of blood clot formation. Annual Review of Fluid Mechanics, 47, 377–403.

Frojmovic MM, Mooney RF, & Wong T (1994). Dynamics of platelet glycoprotein IIb-IIIa receptor expression and fibrinogen binding. I. Quantal activation of platelet subpopulations varies with adenosine diphosphate concentration. Biophys J, 67(5), 2060. [PubMed: 7858143]

Furie B, & Furie BC (2008). Mechanisms of thrombus formation. New England Journal of Medicine, 359(9), 938–949.

Goodman PD, Barlow ET, Crapo PM, Mohammad SF, & Solen KA (2005). Computational model of device-induced thrombosis and thromboembolism. Annals of Biomedical Engineering, 33(6), 780–797. [PubMed: 16078618]

Handin RI (2005). Chapter 53: bleeding and thrombosis. In Harrison's Principles of Internal Medicine (12th ed.). New York: Mcgraw-hill.

Hellums JD (1994). 1993 Whitaker Lecture: biorheology in thrombosis research. Annals of Biomedical Engineering, 22(5), 445–455. [PubMed: 7825747]

Hung TC, Hochmuth RM, Joist JH, & Sutera SP (1976). Shear-induced aggregation and lysis of platelets. ASAIO Journal, 22(1), 285–290.

Ikeda Y, Handa M, Kawano K, Kamata T, Murata M, Araki Y, … Itagaki I (1991). The role of von Willebrand factor and fibrinogen in platelet aggregation under varying shear stress. Journal of Clinical Investigation, 87(4), 1234.

Johnson G, Massoudi M, & Rajagopal KR (1991). Flow of a fluid—solid mixture between flat plates. Chemical Engineering Science, 46(7), 1713–1723.

Johnson G, Rajagopal KR, & Massoudi M (1990). A review of interaction mechanisms in fluid-solid flows(No. DOE/PETC/TR-90/9). USDOE Pittsburgh Energy Technology Center, PA (USA).

Johnston GG, Marzec U, & Bernstein EF (1975). Effects of surface injury and shear stress on platelet aggregation and serotonin release. ASAIO Journal, 21(1), 413–421.

Kang J, Zhang DM, Restle DJ, Kallel F, Acker MA, Atluri P, & Bartoli CR (2016). Reduced continuous-flow left ventricular assist device speed does not decrease von Willebrand factor degradation. The Journal of Thoracic and Cardiovascular Surgery, 151(6), 1747–1754. [PubMed: 26971377]

Kuharsky AL, & Fogelson AL (2001). Surface-mediated control of blood coagulation: the role of binding site densities and platelet deposition. Biophys J, 80(3), 1050–1074. [PubMed: 11222273]

Leiderman K, & Fogelson AL (2011). Grow with the flow: a spatial–temporal model of platelet deposition and blood coagulation under flow. Mathematical Medicine and Biology, 28(1), 47–84. [PubMed: 20439306]

Liang M-L, Da X-W, He A-D, Yao G-Q, Xie W, Liu G, … Ming Z-Y (2015). Pentamethylquercetin (PMQ) reduces thrombus formation by inhibiting platelet function. Scientific Reports, 5, 11142. [PubMed: 26059557]

Lippok S, Radtke M, Obser T, Kleemeier L, Schneppenheim R, Budde U, … Rädler JO (2016). Shear-induced unfolding and enzymatic cleavage of full-length VWF multimers. Biophysical Journal, 110(3), 545–554. [PubMed: 26840720]

Lu Y, Li Q, Liu Y-Y, Sun K, Fan J-Y, Wang C-S, & Han J-Y (2015). Inhibitory effect of caffeic acid on ADP-induced thrombus formation and platelet activation involves mitogen-activated protein kinases. Scientific Reports, 5, 13824. [PubMed: 26345207]

Muthiah K, Connor D, Ly K, Gardiner EE, Andrews RK, Qiao J, … Jarvis S (2016). Longitudinal changes in hemostatic parameters and reduced pulsatility contribute to non-surgical bleeding in patients with centrifugal continuous-flow left ventricular assist devices. The Journal of Heart and Lung Transplantation, 35(6), 743–751. [PubMed: 26987598]

Nesbitt WS, Westein E, Tovar-Lopez FJ, Tolouei E, Mitchell A, Fu J, … Jackson SP (2009). A shear gradient–dependent platelet aggregation mechanism drives thrombus formation. Nature Medicine, 15(6), 665–673.

Netuka I, Kvasnička T, Kvasnička J, Hrachovinová I, Ivák P, Mareček F, … Malý J (2016). Evaluation of von Willebrand factor with a fully magnetically levitated centrifugal continuous-flow left ventricular assist device in advanced heart failure. The Journal of Heart and Lung Transplantation, 35(7), 860–867. [PubMed: 27435529]

OpenCFD. (2011). OpenFOAM Programmer's Guide Version 2.1.0. (OpenCFD, Ed.). Free Software Foundation, Inc.: Boston, MA, USA.

Özkan M, Gündüz S, Gürsoy OM, Karakoyun S, Astarcıoğlu MA, Kalçık M, … Esen AM (2015). Ultraslow thrombolytic therapy: A novel strategy in the management of PROsthetic MEchanical valve Thrombosis and the prEdictors of outcomE: The Ultra-slow PROMETEE trial. American Heart Journal, 170(2), 409–418. [PubMed: 26299240]

Peterson DM, Stathopoulos NA, Giorgio TD, Hellums JD, & Moake JL (1987). Shear-induced platelet aggregation requires von Willebrand factor and platelet membrane glycoproteins Ib and IIb-IIIa. Blood, 69(2), 625–628. [PubMed: 3492225]

Proudfoot AG, Davidson SJ, & Strueber M (2017). State of the art: Von willebrand factor disruption and continuous flow circulatory devices. The Journal of Heart and Lung Transplantation.

Rajagopal KR, & Tao L (1995). Mechanics of mixtures. Series on advances in mathematics for applied sciences (Vol. 35). World Scientific Publishers, Singapore.

Richardson PD (1973). Effect of blood flow velocity on growth rate of platelet thrombi. Nature, 245, 103–104. [PubMed: 4582758]

Ruggeri ZM, & Jackson SP (2013). Platelet thrombus formation in flowing blood. Platelets, 399.

Sakariassen KS, Bolhuis PA, & Sixma JJ (1979). Human blood platelet adhesion to artery subendothelium is mediated by factor VIII–von Willebrand factor bound to the subendothelium. Nature, 279(5714), 636–638. [PubMed: 313016]

Savage B, & Ruggeri ZM (2007). Platelet thrombus formation in flowing blood. Platelets, 359–367.

Schneider SW, Nuschele S, Wixforth A, Gorzelanny C, Alexander-Katz A, Netz RR, & Schneider MF (2007). Shear-induced unfolding triggers adhesion of von Willebrand factor fibers. Proceedings of the National Academy of Sciences, 104(19), 7899–7903.

Skorczewski T, Erickson LC, & Fogelson AL (2013). Platelet motion near a vessel wall or thrombus surface in two-dimensional whole blood simulations. Biophys J, 104(8), 1764–1772. [PubMed: 23601323]

Sorensen EN, Burgreen GW, Wagner WR, & Antaki JF (1999a). Computational simulation of platelet deposition and activation: I. Model development and properties. Ann Biomed Eng, 27(4), 436–448. from http://www.ncbi.nlm.nih.gov/pubmed/10468228 [PubMed: 10468228]

Sorensen EN, Burgreen GW, Wagner WR, & Antaki JF (1999b). Computational simulation of platelet deposition and activation: II. Results for Poiseuille flow over collagen. Ann Biomed Eng, 27(4), 449–458. from http://www.ncbi.nlm.nih.gov/pubmed/10468229 [PubMed: 10468229]

Stalker TJ, Traxler EA, Wu J, Wannemacher KM, Cermignano SL, Voronov R, … Brass LF (2013). Hierarchical organization in the hemostatic response and its relationship to the platelet-signaling network. Blood, 121(10), 1875–1885. [PubMed: 23303817]

Stalker TJ, Welsh JD, Tomaiuolo M, Wu J, Colace TV, Diamond SL, & Brass LF (2014). A systems approach to hemostasis: 3. Thrombus consolidation regulates intrathrombus solute transport and local thrombin activity. Blood, 124(11), 1824–1831. [PubMed: 24951426]

Tomaiuolo M, Stalker TJ, Welsh JD, Diamond SL, Sinno T, & Brass LF (2014). A systems approach to hemostasis: 2. Computational analysis of molecular transport in the thrombus microenvironment. Blood, 124(11), 1816–1823. [PubMed: 24951425]

Tovar-Lopez FJ, Rosengarten G, Westein E, Khoshmanesh K, Jackson SP, Mitchell A, & Nesbitt WS (2010). A microfluidics device to monitor platelet aggregation dynamics in response to strain rate micro-gradients in flowing blood. Lab on a Chip, 10(3), 291–302. [PubMed: 20091000]

Wang W, & King MR (2012). Multiscale modeling of platelet adhesion and thrombus growth. Annals of Biomedical Engineering, 40(11), 2345–2354. [PubMed: 22481228]

Welsh JD, Stalker TJ, Voronov R, Muthard RW, Tomaiuolo M, Diamond SL, & Brass LF (2014). A systems approach to hemostasis: 1. The interdependence of thrombus architecture and agonist movements in the gaps between platelets. Blood, 124(11), 1808–1815. [PubMed: 24951424]

Westein E, van der Meer AD, Kuijpers MJE, Frimat J-P, van den Berg A, & Heemskerk JWM (2013). Atherosclerotic geometries exacerbate pathological thrombus formation poststenosis in a von Willebrand factor-dependent manner. Proceedings of the National Academy of Sciences, 110(4), 1357–1362.

Wu W-T, Aubry N, & Massoudi M (2014). On the coefficients of the interaction forces in a two-phase flow of a fluid infused with particles. International Journal of Non-Linear Mechanics, 59, 76–82.

Wu W-T, Aubry N, Massoudi M, Kim J, & Antaki JF (2014). A numerical study of blood flow using mixture theory. International Journal of Engineering Science, 76, 56–72. [PubMed: 24791016]

Wu W-T, Jamiolkowski MA, Wagner WR, Aubry N, Massoudi M, & Antaki JF (2017). Multi-Constituent Simulation of Thrombus Deposition. Scientific Reports, 7, 42720. [PubMed: 28218279]

Wu W-T, Yang F, Antaki JF, Aubry N, & Massoudi M (2015). Study of blood flow in several benchmark micro-channels using a two-fluid approach. International Journal of Engineering Science, 95, 49–59. [PubMed: 26240438]

Wurzinger LJ, Opitz R, Blasberg P, & Schmid-Schönbein H (1985). Platelet and coagulation parameters following millisecond exposure to laminar shear stress. Thrombosis and Haemostasis, 54(2), 381–386. [PubMed: 2934855]

Wurzinger LJ, Opitz R, Wolf M, & Schmid-Schönbein H (1984). "Shear induced platelet activation"--a critical reappraisal. Biorheology, 22(5), 399–413.

Xu Z, Chen N, Kamocka MM, Rosen ED, & Alber M (2008). A multiscale model of thrombus development. Journal of the Royal Society Interface, 5(24), 705–722.

Xu Z, Lioi J, Mu J, Kamocka MM, Liu X, Chen DZ, … Alber M (2010). A multiscale model of venous thrombus formation with surface-mediated control of blood coagulation cascade. Biophys J, 98(9), 1723–1732. [PubMed: 20441735]

Zhao R, Marhefka JN, Shu F, Hund SJ, Kameneva MV, & Antaki JF (2008). Micro-flow visualization of red blood cell-enhanced platelet concentration at sudden expansion. Annals of Biomedical Engineering, 36(7), 1130–1141. [PubMed: 18418710]

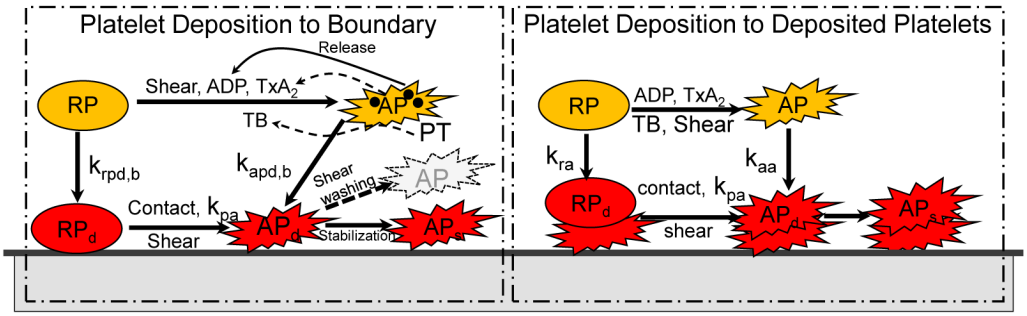


**Figure 1.**

Schematic depiction of the thrombosis model, comprised of platelet deposition, aggregation, and stabilization. [RP]: resting platelet, [AP]: activated platelet, [$RP_d$] and [$AP_d$]: deposited resting and activated platelets, [$AP_s$]: stabilized deposited activated platelets. Agonists that cause activation ([RP] to [AP]) are adenosine diphosphate, ADP; thromboxane $A_2$, $TxA_2$; shear, and thrombin, TB – which is synthesized from prothrombin (PT). The suffix b refers to the reaction with the boundary (surface.)

The constants $k_{pa}$, $k_{ra}$, $k_{aa}$, $k_{rpd,b}$, $k_{apd,b}$, refer to the reaction rates for inter-conversion of the associated platelet states.

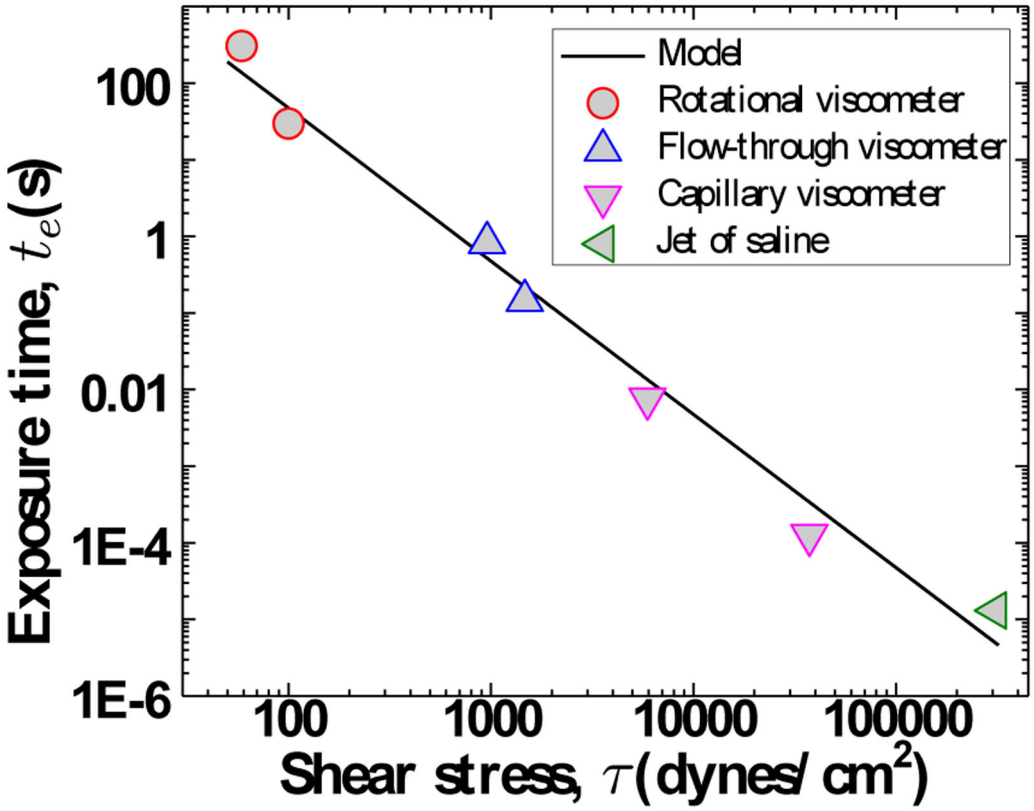


**Figure 2.**

Exposure time needed for platelets activation as a function of shear stress, based on multiple experiments: in parallel plates (Hellums, 1994), in rotational viscometer (Anderson et al., 1978, 1977; Brown III et al., 1975; Hung et al., 1976), flow-through viscometer (Wurzinger et al., 1985, 1984), capillary viscometer (Colantuoni et al., 1977) and jet (Johnston et al., 1975).

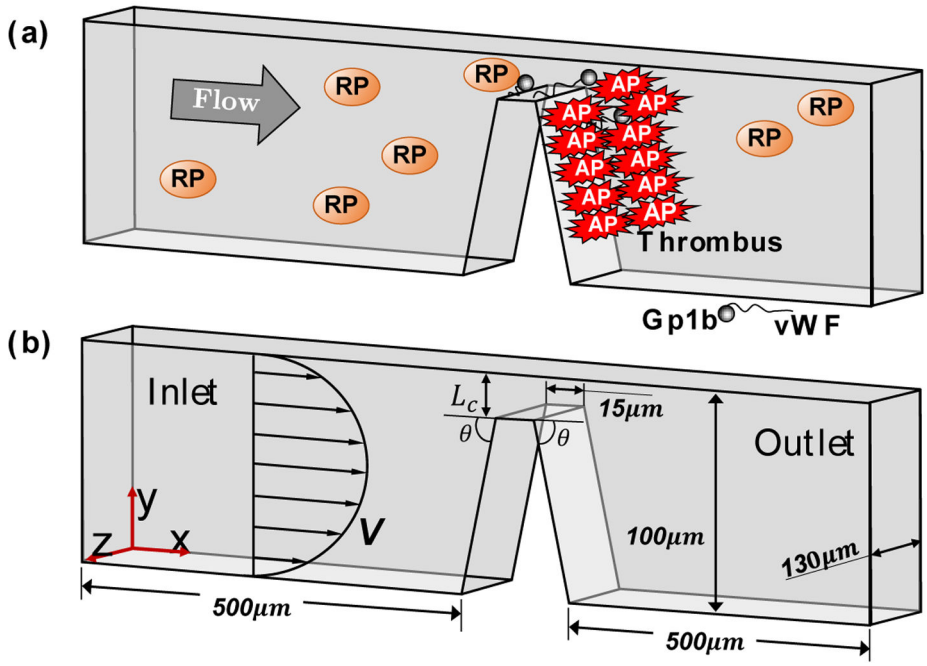


**Figure 3.**

(a) Schematic of the processes of vWF unfolding, capture of resting platelets ([RP]), and activation by exposure to shear in a stenosis channel. (b) Parameterized, idealized stenosis used in this simulation.

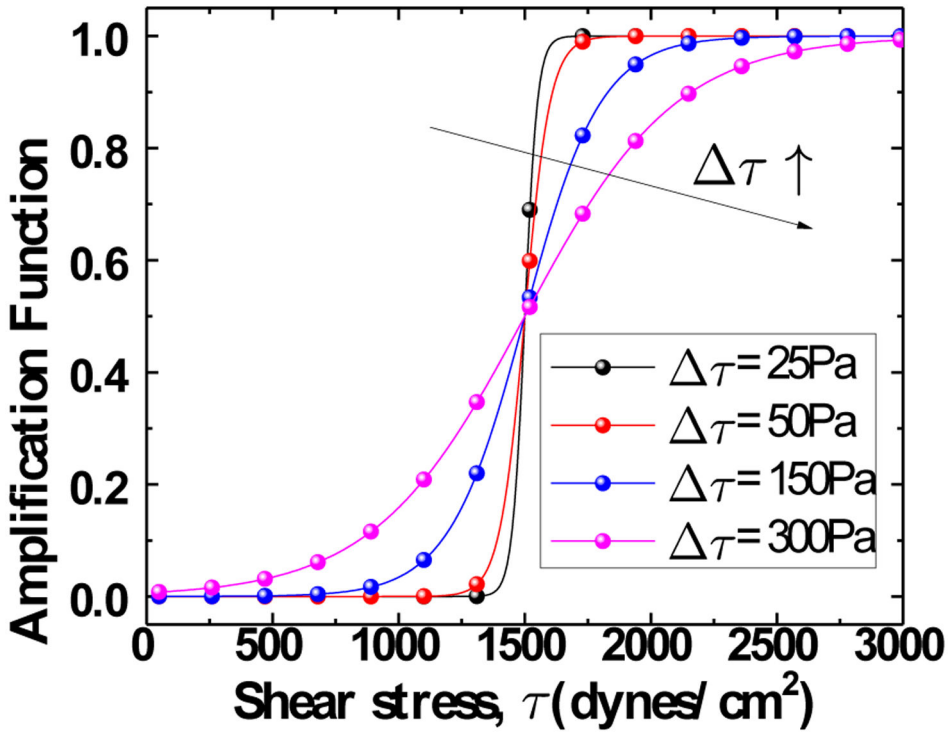


**Figure 4.**
vWF amplification function, $f_{vWF}$, as a function of shear stress, when the constant $C_{vWF} = 1$.

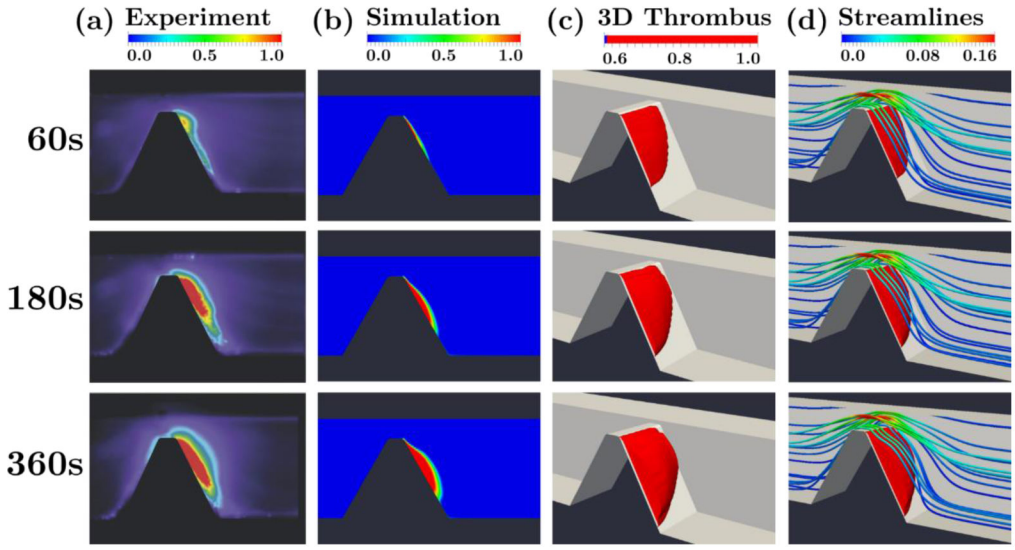


**Figure 5.**

Deposition of platelets in x-y cross section at z-position of 30$\mu m$ observed experimentally (a) (Tovar-Lopez et al., 2010) (used by permission) and by numerical simulations (b), averaged in the z-direction to account for the finite depth-of-field of the experimental images, assumed to be 10$\mu m$ (Wu et al., 2015; Zhao et al., 2008). (c) Sectional view of 3D rendering of the simulated thrombus. (d) Streamlines distorted by thrombus. (Units of the scale bar are $m/s$.) The expansion angle is $\theta = 60°$.

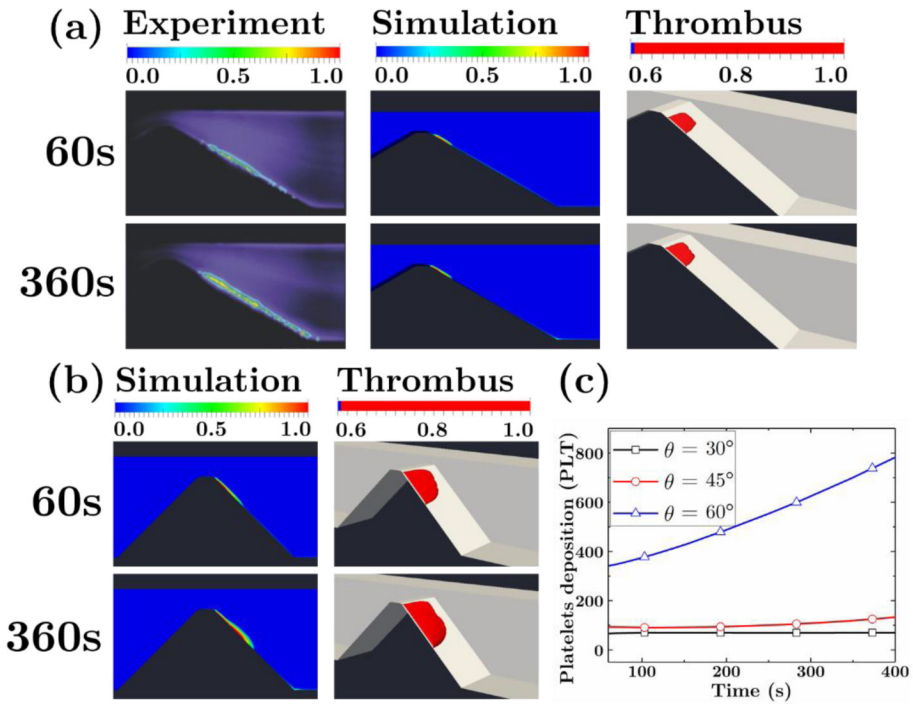


**Figure 6.**

(a) Platelet deposition in x-y cross section at z-position of 30μm for expansion angle of $\theta$ = 30°. Experimentally measured volume fraction (Tovar-Lopez et al., 2010) (left) compared to simulation (center) and 3D rendering of the simulated thrombus (right). (b) The volume fraction field of the platelets (left) and 3D rendering of the thrombus (right) by the numerical simulation for $\theta$ = 45°. (c) Platelets deposition (count) versus time illustrating effect of angle on growth rate. The experimental data in (a) were used by permission.

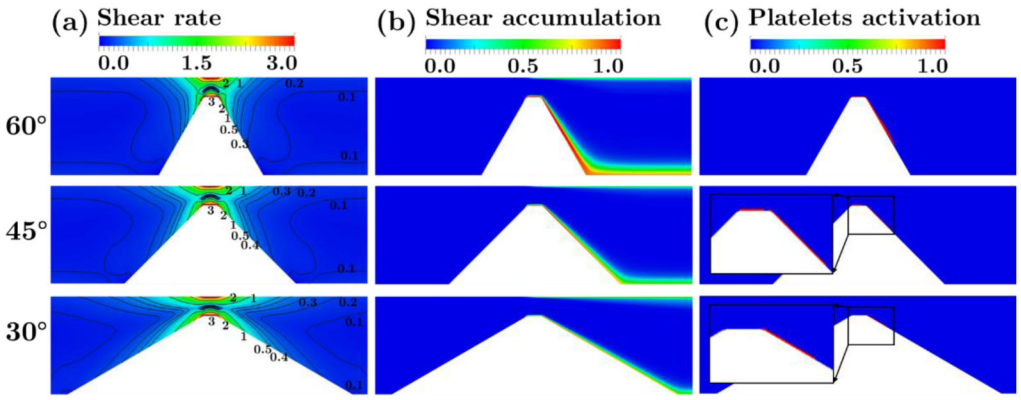


**Figure 7.**

(a) Shear field, (b) shear stress accumulation and (c) platelets shear activation field in x-y cross section at z-position of 30μm with different expansion angles, $\theta = 60°, 45°, 30°$. The Reynolds number is 0.70. All the fields are shown at t=1s (at the beginning of the simulations). The units of scale bars of figure (a) and figure (b) are $10^4 s^{-1}$ and $kg \cdot m^{-1} \cdot s^{-1}$, respectively.

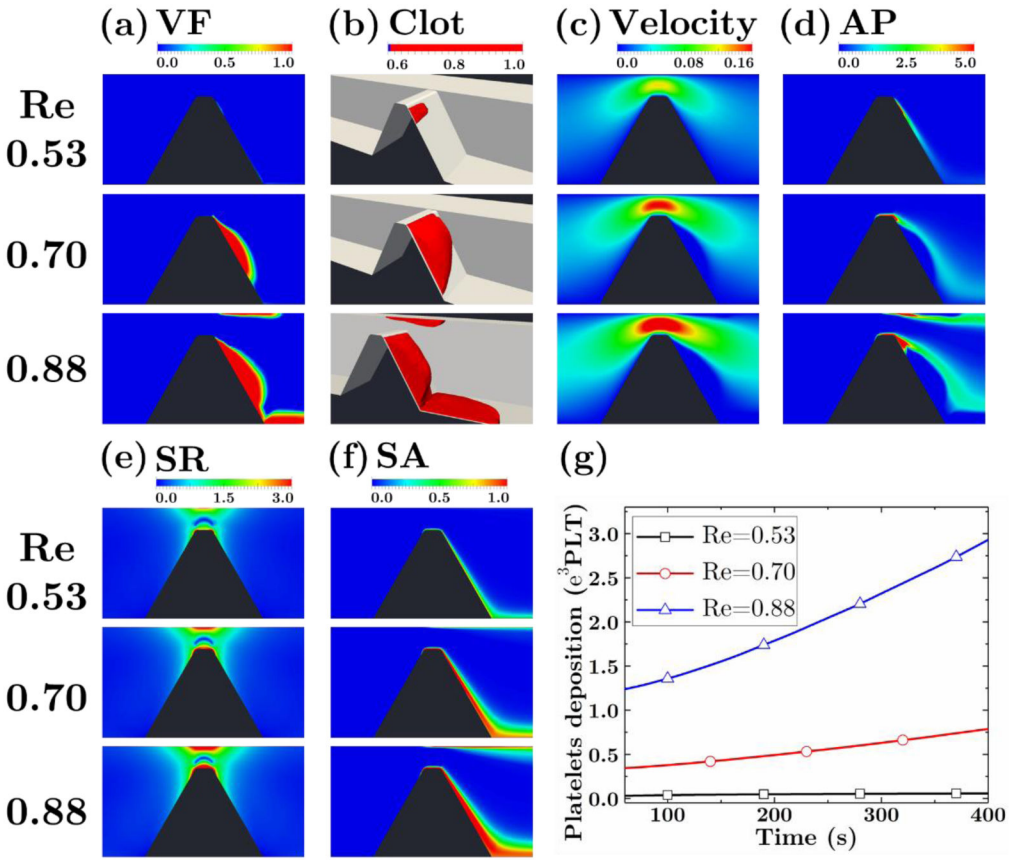


**Figure 8.**

Effect of flow rate (Reynolds number). Distributions of (a) platelet deposition, (b) 3D rendering of the thrombus, (c) velocity, (d) activated platelets (in flow), (e) shear rate, (f) shear stress accumulation, and (g) platelet accumulation vs time. All the two-dimensional fields are from x-y cross section at z-position of 30μm. Figure (a)-(d) are captured at t=360s, while figure (e) and (f) are obtained at t=1s. The units of scale bars of figure (c), (d), (d) and (f) are $m \cdot s^{-1}$,$10^{13} PLT \cdot m^{-3}$, $10^4 s^{-1}$ and $kg \cdot m^{-1} \cdot s^{-1}$.

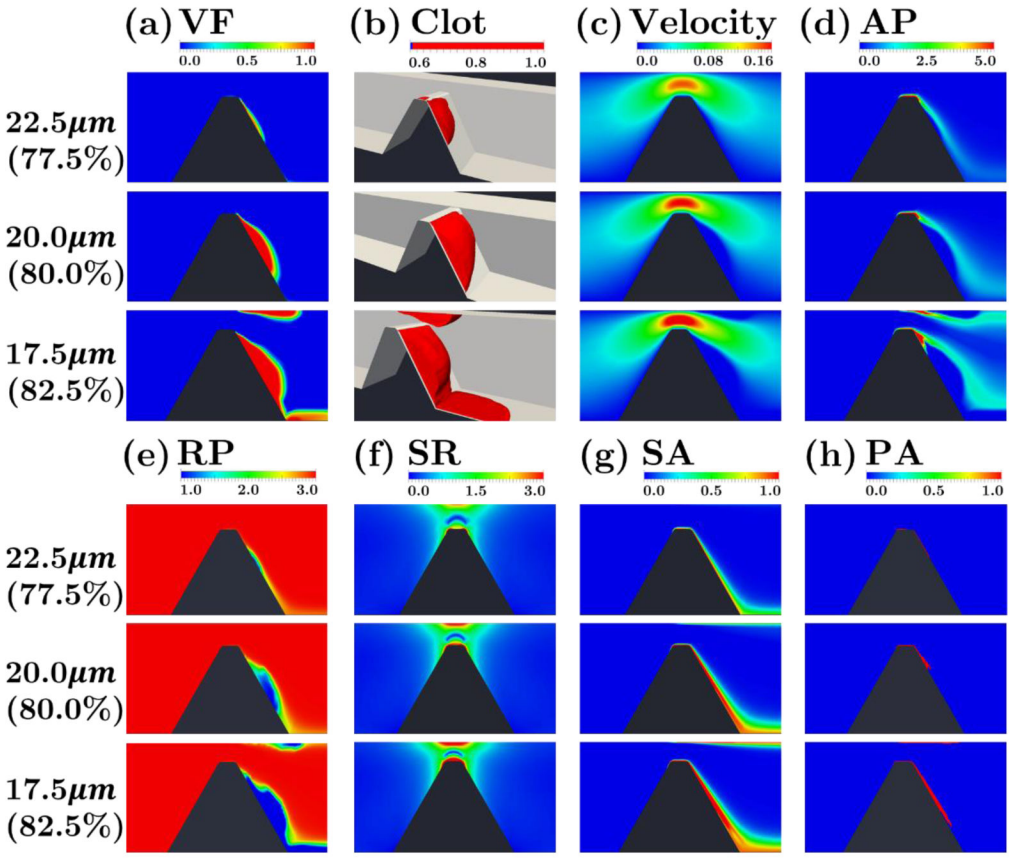


**Figure 9.**

Effect of degree of stenosis on distributions of (a) platelet deposition, (b) 3D rendering of the thrombus, (c) velocity, (d) activated platelets (in flow), (e) resting unactivated platelets, (f) shear rate, (g) shear stress accumulation, and (h) platelets shear activation. All the two-dimensional fields are from x-y cross section at z-position of 30μm. Figure (a)-(e) are acquired at t=360s, while figure (f), (g) and (h) are provided for t=1s. The units of scale bars of figure (c), (d), (e), (f) and (g) are $m \cdot s^{-1}$,$10^{13} PLT \cdot m^{-3}$, $10^{14} PLT \cdot m^{-3}$, $10^{4} s^{-1}$ and $kg \cdot m^{-1} \cdot s^{-1}$.

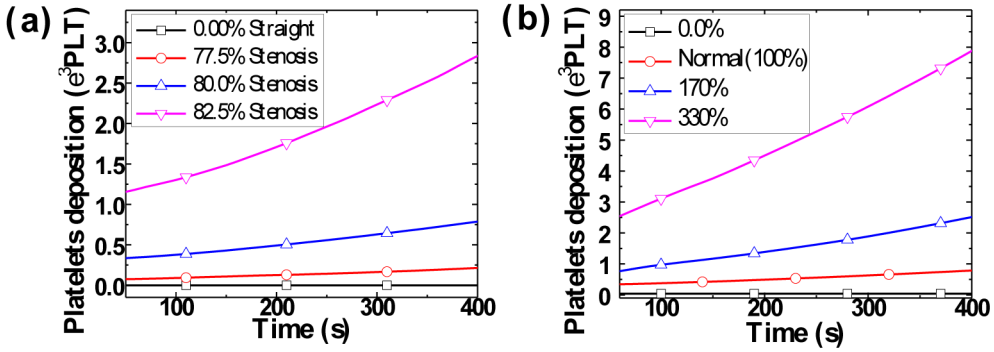


**Figure 10.**

Platelet accumulation as a function of time with (a) different degrees of stenosis and (b) different vWF activity.